C/ORNL95-0363

ornl

OAK RIDGE NATIONAL LABORATORY

LOCKHEED MARTIN

CRADA Final Report
for
CRADA Number ORNL95-0363

METAL COMPRESSION FORMING OF ALUMINUM ALLOYS AND METAL MATRIX COMPOSITES

S. Viswanathan, W. Ren, W. D. Porter,
C. R. Brinkman, and A. S. Sabau
Oak Ridge National Laboratory
Oak Ridge, Tennessee

R. M. Purgert
Thompson Aluminum Casting Co.
Cleveland, Ohio

APPROVED FOR PUBLIC RELEASE

UNLIMITED DISTRIBUTION

MANAGED AND OPERATED BY
LOCKHEED MARTIN ENERGY RESEARCH CORPORATION
FOR THE UNITED STATES
DEPARTMENT OF ENERGY

ORNL-27 (3-96)

DISCLAIMER

DISCLAIMER

Portions of this document may be illegible in electronic image products. Images are produced from the best available original document.

CONTENTS

Abstract

Metal Compression Forming (MCF) is a variant of the squeeze casting process, in which molten metal is allowed to solidify under pressure in order to close porosity and form a sound part. However, the MCF process applies pressure on the entire mold face, thereby directing pressure on all regions of the casting and producing a uniformly sound part. The process is capable of producing parts with properties close to those of forgings, while retaining the near net shape, complexity in geometry, and relatively low cost of the casting process. The paper describes the casting process development involved in the production of an aluminum A357 alloy motor mount bracket, including the use of a filling and solidification model to design the gating and determine process parameters. Tensile properties of the component are presented and correlated with those of forged components. Limited fatigue properties obtained by fully reversed strain controlled testing are presented. The results indicate that the MCF process is commercially viable for the manufacture of high-integrity structural components of aluminum alloys. Results are also presented on casting trials, the resulting microstructure, and tensile properties of Duralcan metal matrix composite (MMC) alloy. The MCF process appears to be a promising route for the manufacture of MMC components, although further development of melting and mold filling procedures are needed fore commercial implementation.

CRADA Objective

The objective of this Cooperative Research and Development agreement (CRADA) project involving Thompson Aluminum Casting Co. (TAC) and Oak Ridge National Laboratory (ORNL) was to demonstrate Metal Compression Forming (MCF) as a cost-effective, high-integrity, environmentally responsible, net-shape casting process for aluminum alloys and metal matrix composites (MMCs). The MCF process, a variant of the squeeze casting process, is designed to allow the manufacture of pore-free cast aluminum alloy components with properties comparable to forged parts, at considerably lower cost. This allows cast aluminum alloy parts to be used in safety-critical structural applications requiring high tensile strength and ductility, and importantly, high fatigue strength, particularly for automotive and truck applications. In this CRADA, computer modeling of the MCF process was carried out to aid process development and optimization. MCF parts were characterized by optical microscopy, scanning electron microscopy (SEM), and X-ray computer tomography (CT), to study the microstructure, and the shape and distribution of defects. Tensile and fatigue testing of MCF components was carried out to check and demonstrate the suitability of MCF components for safety-critical structural applications.

Assessment of CRADA

The results of the modeling and experimental studies undertaken in this CRADA successfully demonstrated the ability of the MCF process to produce pore-free net-shape cast components of A356 aluminum alloy with properties comparable to wrought 6061 aluminum alloy samples. A prototype A356 motor mount bracket was produced as a

demonstration component in the CRADA. The motor mount bracket was tested by an automotive company and qualified as a replacement for a forged 6061 aluminum alloy part. Based on these results, the MCF process was awarded an R&D 100 Award by *R&D Magazine* in 1997, recognizing it as one of the 100 most technologically significant new products of the year.

In addition, based on the results of the casting modeling carried out for the prototype phase of the project, a commercial version of the MCF process was developed. The commercial version of the MCF process further improved metal delivery and casting yield over the prototype version of the process. Licensing of the MCF process to automotive suppliers is currently being negotiated. The MCF process was also used to produce components of an MMC alloy and 6061 aluminum alloy. However, although the MCF process was deemed promising for the production of MMC and 6061 alloy components, the development of the MCF process for the production of MMC and 6061 alloy were not completed before the conclusion of the CRADA.

CRADA Benefit to DOE

This CRADA has enhanced the capabilities and skills at the Oak Ridge National Laboratory (ORNL) in the areas of casting process design, process modeling, simulation of heat and fluid flow, and the prediction of microporosity in castings. This will improve the prospects of future projects on the processing of advanced materials. The project has also allowed ORNL to obtain information on a casting process for producing premium quality castings that could be applied to the commercialization of alloys developed in DOE programs.

The CRADA also successfully demonstrated the application of DOE technologies in the areas of casting solidification and process modeling to the solution of problems encountered in production castings in a commercial foundry. It also demonstrated that DOE programs can allow small businesses to access the technology available at DOE laboratories. Finally, the project has resulted in the development of an advanced casting technology for the production high-integrity, cost-effective, lightweight alloy components that can replace steel and cast iron in automotive and truck applications, resulting in energy and environmental benefits.

Technical Discussion

The use of aluminum alloy castings for safety critical structural components such as engine mount brackets, steering knuckles, and control arms, offers significant opportunities for achieving weight reduction in automobiles, since they are typically about half the weight of the steel, cast iron, or ductile iron component that they replace. Unfortunately, most cast aluminum alloy components contain dispersed porosity resulting from shrinkage of the alloy during solidification and from the precipitation of gas, as well as oxide films and trapped gas from turbulence during filling of the mold cavity, limiting their ductility and fatigue strength and making them unsuitable as safety critical structural

components. The Metal Compression Forming (MCF) process, a variant of the squeeze casting process, allows the manufacture of aluminum alloy components that are relatively free of porosity and oxide skin defects, resulting in properties comparable to forged parts. This allows cast aluminum alloy parts to be used in safety critical structural applications requiring high tensile strength and ductility, and importantly, high fatigue strength, particularly for automotive applications.

Formation of Porosity in Castings

Porosity can be broadly classified into two types, namely, macroporosity, also termed shrinkage pipe or centerline shrinkage, and microporosity, also described as interdendritic porosity or porosity that cannot easily be discerned by the naked eye. Macroporosity is strongly affected by the casting geometry and thermal conditions, and can be eliminated by adequate feeding or risering. Microporosity, on the other hand, results due to a combination of shrinkage and gas evolution and is dispersed and usually microscopic. Microporosity cannot be eliminated by feeding or risering alone. It can only be eliminated by also controlling the amount of dissolved gas in the molten alloy and by the application of pressure during solidification. Microporosity can markedly reduce mechanical properties, in particular ductility and fatigue properties, even when present in fairly small amounts. It is microporosity that is of primary interest and of concern in this project.

The formation and distribution of porosity in a solidifying alloy is dependent on the mode of solidification. The mode of solidification of an alloy, from the considerations of the feeding of solidification shrinkage, primarily depends on the freezing range of the alloy and its thermal conductivity. The freezing range of the alloy determines the temperature range over which the alloy is in a "mushy" stage. In an alloy such as aluminum alloy with high thermal conductivity, thermal gradients are likely to be low; points that are widely spaced in a casting are likely to be at the same or similar temperature and fraction solid. Castings of alloys of high thermal conductivity and a large freezing range such as aluminum alloys are mushy over the entire solidification process, and fluid flow to feed shrinkage takes place through long, tortuous, interdendritic channels. The combination of the relatively high resistance to the flow of liquid metal through tortuous flow channels and the precipitation of dissolved gas in the liquid metal, usually hydrogen, toward the end of solidification, results in the formation of dispersed microscopic porosity, or microporosity. Figure 1 illustrates mushy solidification in many aluminum alloys.

The Metal Compression Forming Process

The formation of gas porosity cannot usually be avoided in traditional gravity assisted casting processes. In addition, in both gravity assisted filling or during rapid metal injection such as in high pressure die casting, trapped gas and oxide films are introduced into the casting during the filling of the mold cavity, creating defects that cause castings to fail prematurely under cyclic loading. The MCF process can use low-pressure bottom-filling to allow the filling of the mold cavity in a quiescent manner and avoid the

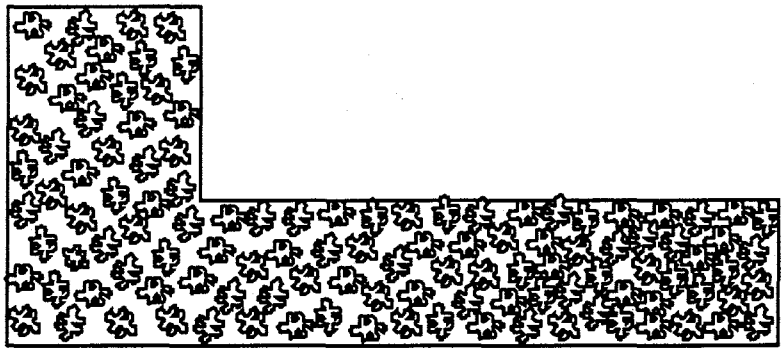

Fig. 1. Mushy solidification typical of aluminum alloys.

formation of trapped gas pockets and oxide films. In addition, in the MCF process, molten metal is allowed to solidify under pressure in order to close porosity and form a sound part. The MCF process applies pressure on the entire mold face, thereby directing pressure uniformly on all regions of the casting and producing a uniformly sound part.

Processes such as indirect squeeze casting that apply pressure on the gate area via a plunger also use pressure during solidification to eliminate porosity. However, parts made by the indirect squeeze casting process may be sound near the gate where pressure is applied, but may exhibit higher levels of porosity away from the gate, making certain areas of the casting weaker than others. In addition, the introduction of molten metal into a cavity by the use of a plunger promotes turbulent flow during filling, and creates trapped gas pockets and oxide films that weaken the casting. Figure 2 shows a schematic of the indirect squeeze casting process, and the expected non-uniform pressure distribution during solidification. Figure 3 shows a schematic of the MCF process, and the expected uniform pressure distribution during solidification. Due to the application of uniform pressure over the entire casting, the MCF process is capable of producing parts with uniformly superior mechanical properties close to those of forgings, while retaining the near net shape, complexity in geometry, high throughput, and relatively low cost of the die casting process.

Project Description and Results

The purpose of the CRADA project involving TAC and ORNL was to demonstrate that MCF was a cost-effective, high-integrity, environmentally responsible, net-shape casting process for aluminum alloys and metal matrix composites (MMCs). As part of the development and optimization of the MCF process for the production of A356 aluminum alloy motor mount brackets, computer modeling of the MCF process was carried out to aid process development and optimization. MCF parts were characterized by optical microscopy, scanning electron microscopy (SEM), and x-ray computer tomography (CT) to study the microstructure, and the shape and distribution of defects. Tensile and fatigue testing of MCF components were carried out to check and demonstrate the suitability of MCF components for safety-critical structural applications.

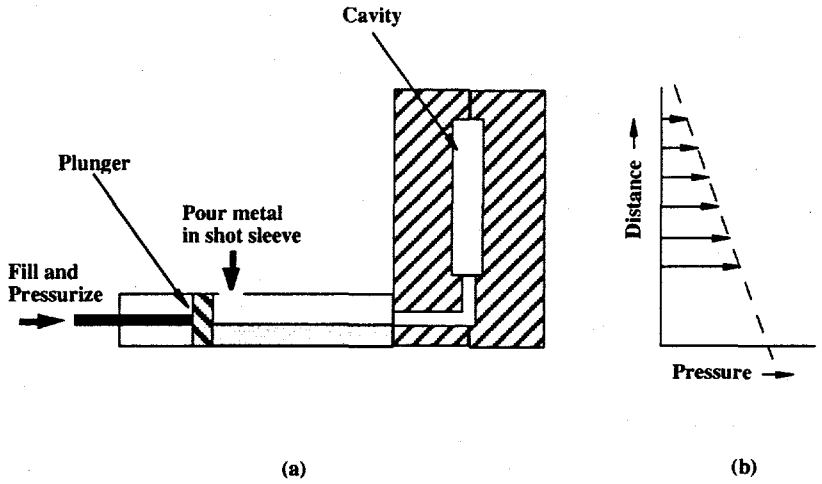

Fig. 2. Schematic illustration of the indirect squeeze casting process showing: (a) the starting position in which the dies are engaged and metal has been poured into the shot sleeve, and (b) the resulting nonuniform pressure profile in the die cavity when the plunger is moved to inject the die with molten metal and simultaneously pressurize the metal in the die cavity from one end.

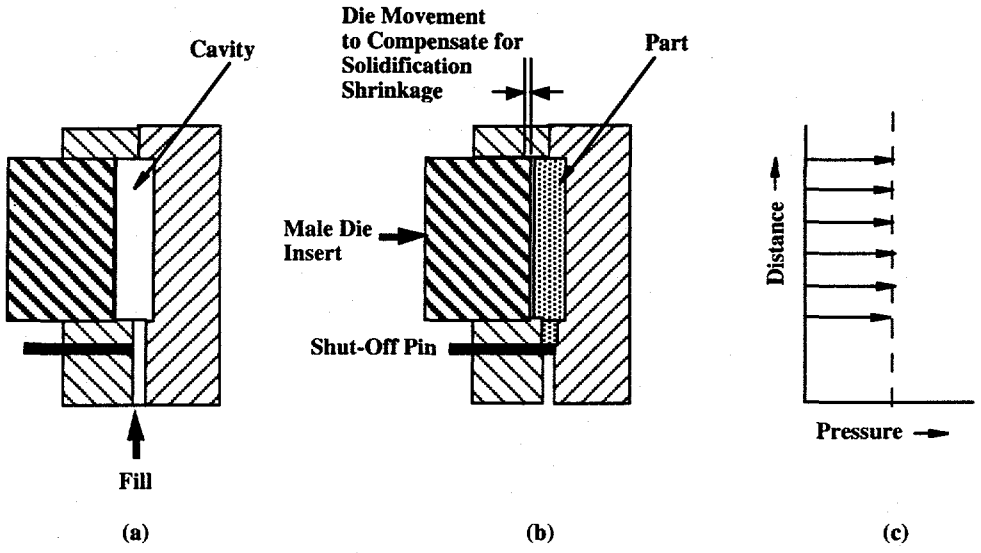

Fig. 3. Schematic illustration of the Metal Compression Forming process showing: (a) the starting position in which the dies are engaged but the shut-off pin is withdrawn for filling, (b) the end position in which the shut-off pin has been engaged and the cavity has been pressurized by the movement of the male die, and (c) resulting uniform pressure profile in the die cavity.

Production of Test Bar

Prior to the casting process development required for production of the motor mount bracket, a test bar was produced for the purpose of determining tensile properties and verifying the capability of the process. For the production of the test bar casting, TAC decided to use a tilt pour arrangement to fill the die in order to minimize turbulence, prevent air entrapment, and consequently allow castings to be heat-treated. A 250-ton die casting machine was modified to allow the platen to rotate 90° in the plane of the platens and allow tilt pour filling of the test bar die. The shot sleeve was removed. One of the platens was fixed and contained the female half of the die. The other platen was movable and contained the male half of the die. The parting line was parallel to the platens as in a typical die casting die and the die cavity was filled from the side using a pouring cup. At the start of the process, the male and female halves of the die were engaged to provide a closed cavity. Molten metal was ladled into the pouring cup, and the platens and dies were rotated to allow the metal to fill the die. On completion of filling, a hydraulically actuated shut-off pin shut off the sprue and the movement of the male half of the die pressurized the mold cavity. Pressurization continued till the end of solidification, after which the male die was retracted and the part ejected. Mold coolant and lubricant were applied after part ejection and the cycle was repeated. Figure 4 shows an external view of the MCF machine used in this effort.

The test bar die produced a flat tensile specimen of nominal dimensions 12 × 12 × 90 mm in the gauge section and 18 × 12 × 50 mm in the grip section. For the production of the test bar, no grain refiner or strontium modifier was added to the melt, nor was the melt degassed. Thus, the results obtained should be fairly conservative. Figure 5 shows a photograph of the test bar. As shown in Fig. 5, the actuation of the shut-off pin effectively isolated the die cavity from the open sprue and essentially cut the part off at that point. A contraction was provided at the gate below the shut-off pin to allow the test bar to be easily broken or cut off at the gate area. Figure 6 shows an X-ray computer tomography radiograph of the test bar. It shows the test bar to be completely sound in the gauge section. A small amount of porosity was visible in the grip section, indicating that further optimization of the process was required for porosity to be completely eliminated. Figure 7 shows an optical micrograph of the microstructure in the test bar. It indicates that the high cooling rate obtained in the MCF process produced a high level of refinement of the eutectic silicon even in the absence of strontium addition. The high cooling rate also resulted in a fairly fine dendrite cell spacing of approximately 35 μm.

Specimens were machined from the gauge section of the test bar for tensile tests at -40°C, room temperature, and 120°C. Cylindrical specimens with a gauge length of 28.6 mm (1.125 in.) and a diameter of 3.2 mm (0.125 in.) in the gauge section and 6.4 mm (0.25 in.) in the grip section were used for all tensile tests. Tensile tests at -40°C and 120°C were conducted in an insulated environmental chamber. A fan circulated air in the chamber to maintain constant temperature. For the -40°C tests, liquid nitrogen was used to cool the circulated air, while for the 120°C tests a resistant heating element was employed to heat the circulated air. The liquid nitrogen flow and the heating element were controlled by a thermocouple tied directly to the specimen.

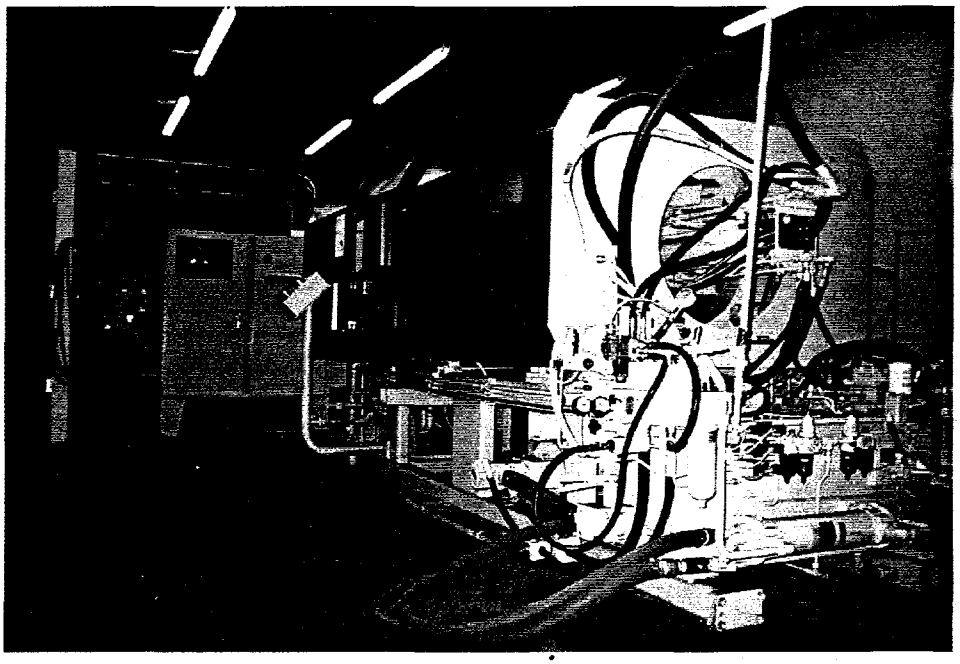

Fig. 4. External view of modified die casting machine used for metal compression forming of the prototype motor mount bracket.

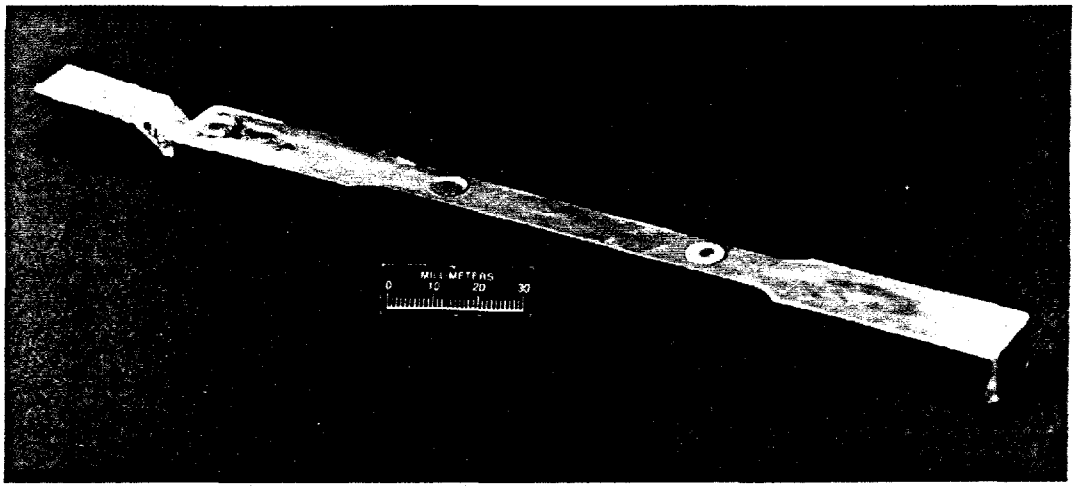

Fig. 5. Photograph of test bar produced by metal compression forming.

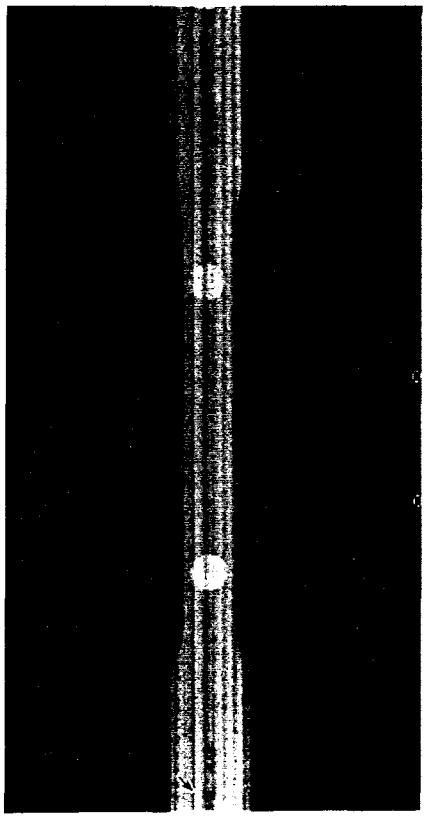

Figure 6. Computer tomography radiograph of Metal Compression Formed Test Bar.

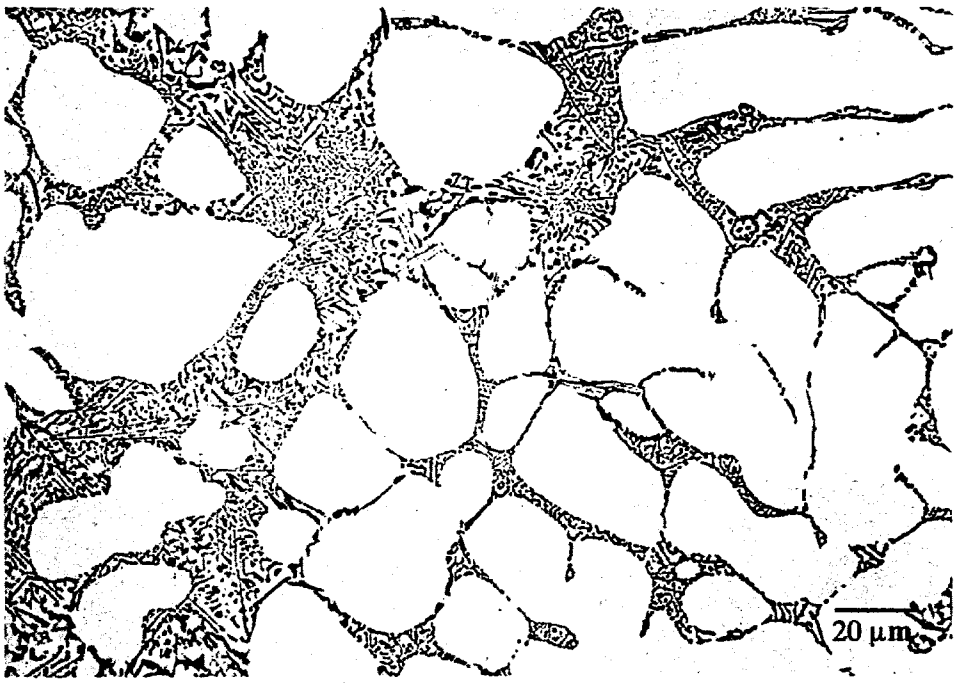

Figure 7. Optical micrograph of Metal Compression Formed test bar.

Figure 8 shows a plot of ultimate and yield strengths measured from specimens obtained from the MCF test bar. For purposes of comparison, ultimate and yield strengths for wrought and squeeze cast 6061 alloy and for squeeze cast 356 alloy obtained from the ASM Casting Handbook are also shown.

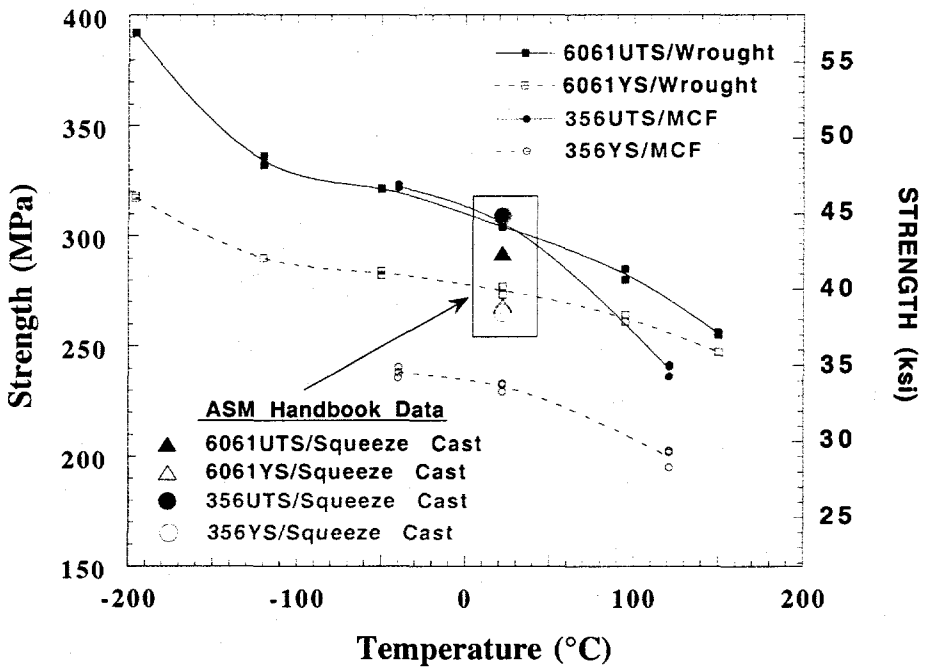

Figure 8. Plot of ultimate and yield strengths measured from specimens obtained from metal compression formed test bar. Also shown are values for wrought 6061 and squeeze cast 6061 and 356 alloys for comparison.

The data clearly demonstrated that the ultimate tensile strength values for the MCF samples compared favorably with those for the wrought and squeeze cast 6061 and 356 alloy samples. The yield strength exhibited by the MCF samples was lower than for either the wrought or squeeze cast samples. However, it was assumed that this difference was due to a difference in heat treatment as well due to the fact that no special efforts were made to control the alloy composition for the production of the test bar castings.

Figure 9 shows a plot of the tensile elongation for specimens obtained from the MCF test bar. Again, values for wrought and squeeze cast 6061 alloy and squeeze cast 356 alloy are also plotted for comparison. The data indicate that the properties for the MCF specimens compare favorably to the data for wrought and squeeze cast 6061 alloy specimens and significantly exceed the published data for squeeze cast 356 alloy, although in this case the published data for squeeze cast 356 alloy seem to be rather low. However, the fact that tensile elongation values of nearly 12% were achieved for 356 alloy indicates that microporosity in the samples was extremely low or absent. Metallographic examination of the test bars did not indicate any evidence of microporosity.

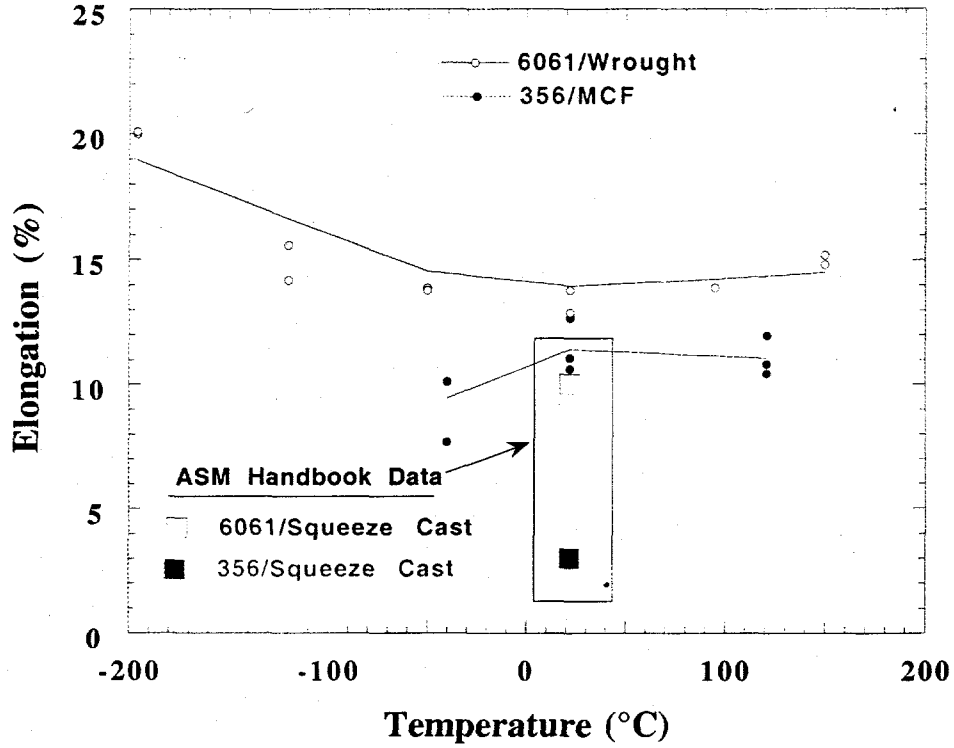

Figure 9. Plot of tensile elongation measured from specimens obtained from Metal Compression Formed test bar. Also shown are values for wrought 6061 and squeeze cast 6061 and 356 alloys for comparison.

Initial Trials of Motor Mount Bracket

The tensile properties obtained from the MCF test bar confirmed that the process was capable of producing properties close to that of forging. The development of the MCF process for the prototype production of the motor mount bracket consisted of the design of the die including the modeling of the filling of the die cavity and the subsequent solidification of the part. For the prototype production of the motor mount bracket, TAC decided to use the same tilt pour arrangement used in the production of the test bar described in the previous section. Figure 10 provides a close-up of the dies used for the prototype production of the motor mount bracket.

The die cavity configuration was designed with two cavities one on top of another. Figure 11 shows a photograph of the initial gating system with a bracket attached to the top cavity. Casting trials using this gating system produced castings that exhibited severe surface defects. Figure 12 shows a bracket from the upper cavity produced using the initial gating system design. The source of the surface defects was unclear, although solidification shrinkage was suspected. Accordingly, it was decided to model the tilt pour filling of the die and subsequent solidification of the motor mount.

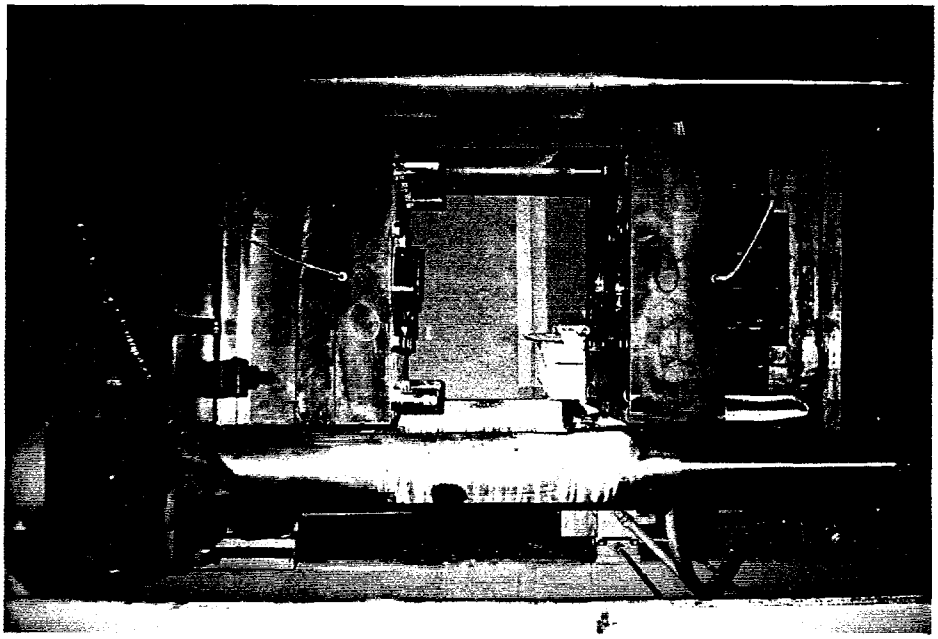

Fig. 10. Close-up of dies used for prototype production of motor mount bracket by metal compression forming.

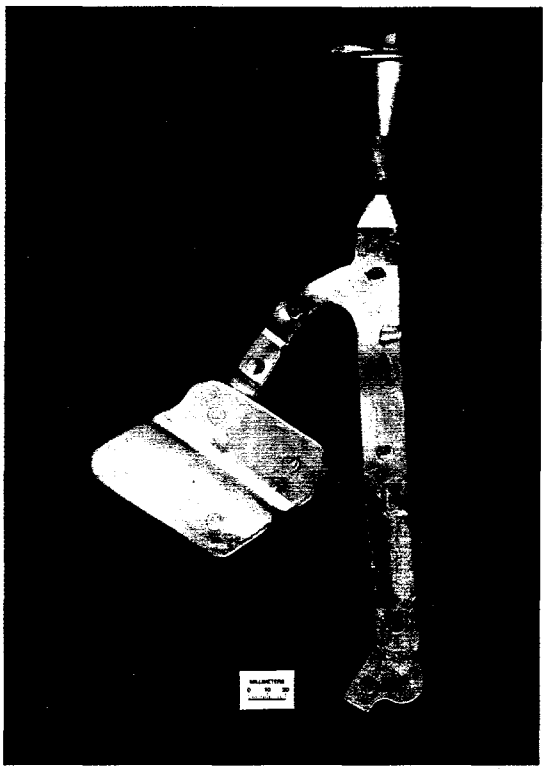

Fig. 11. The initial gating system design indicating a down-sprue and two cavities set one on top of the other. Only the bracket attached to the upper gate is shown in this figure.

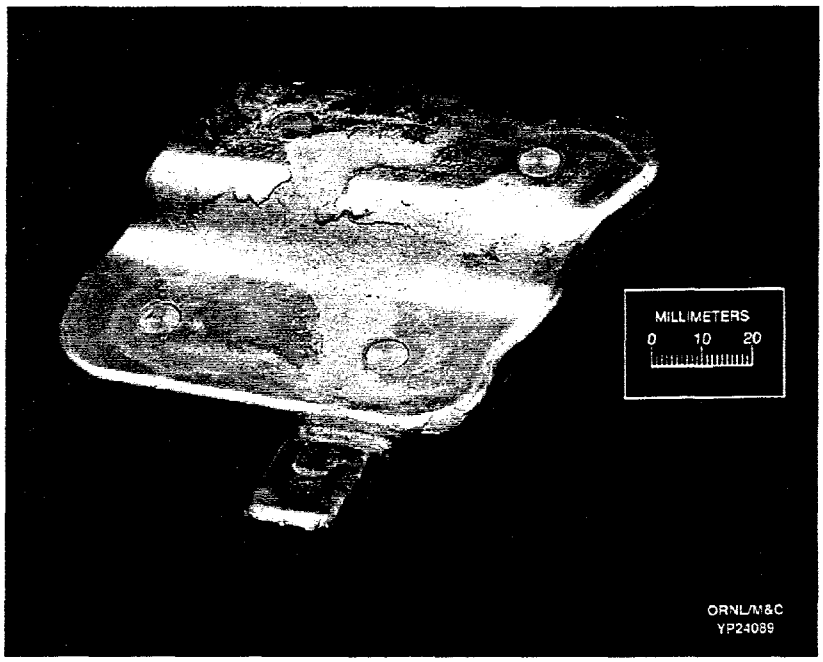

Fig. 12. Motor mount bracket produced using the initial gating system design exhibiting severe surface defects.

Measurement of Thermophysical Properties for Modeling

Thermophysical properties were determined at the facilities of the High Temperature Materials Laboratory (HTML) at ORNL. Thermal conductivity (K) was determined by its relation to thermal diffusivity (α), bulk density (ρ), and specific heat (C_P), by $K = \alpha\rho C_P$. Thermal diffusivity was determined using the laser flash thermal diffusivity technique (LFTD). Specific heat capacity was measured using differential scanning calorimetry (DSC). Linear thermal expansion (LTE) and density were determined by high-temperature dilatometry. A dual push-rod differential dilatometer equipped with a thermally isolated linear variable displacement transducer (LVDT) was used to accurately measure displacement as a function of temperature. For density measurements, the dilatometer was operated in a single push-rod configuration outfitted with a special POCO™ graphite tube and end caps which contained the alloy sample during melting (see Figure 13). The alloy specimen was then heated to 800°C and cooled to below its solidification temperature (500°C). The change in length was measured and multiplied by the cross sectional area of the specimen to determine the volume change during solidification, after compensating for the thermal expansion of the system. The density was calculated over this temperature range from the mass of the specimen. Table 1 lists the measured thermophysical properties for the alloy as a function of temperature.

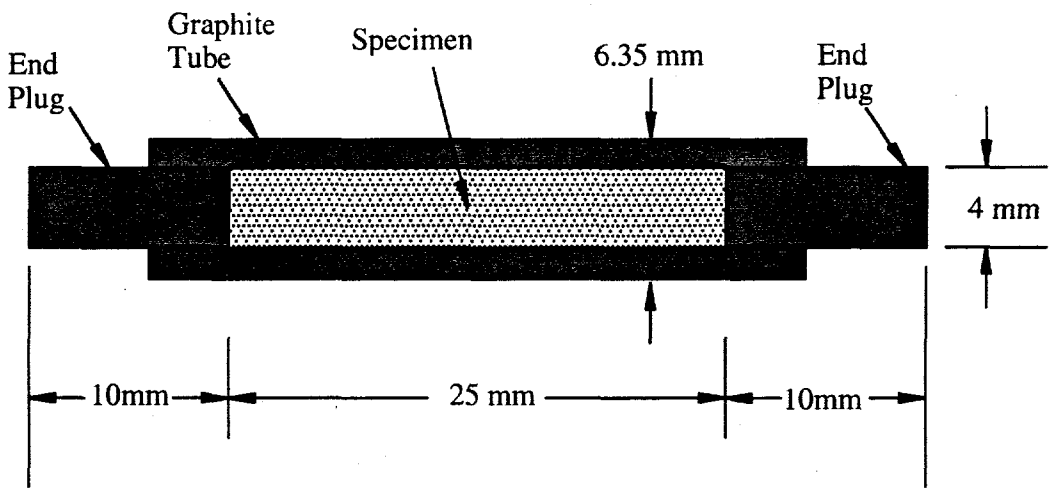

Fig. 13. Schematic of modified push-rod arrangement used for density measurement by dilatometry.

Table 1. Measured thermophysical properties for aluminum 356 alloy used in modeling

Temperature (°C)	Thermal Conductivity (W/m/K)	Density (g/cc)	Specific Heat (KJ/Kg/K)
25		2.67	
100	160.78		0.95718
125	163.08		0.9685
150	165.96		0.97982
175	169.23		0.99114
200	172.70		1.0025
225	176.14		1.0138
250	179.36		1.0251
275	182.18		1.0364
300	184.43		1.0477
325	186.00		1.0591
350	186.81		1.0704
375	186.87		1.0817
400	186.23		1.093
425	185.05		1.1043
450	183.59		1.1157
475	182.22		1.127
500	181.44		1.1383
560		2.56	
615		2.42	
800		2.37	

Latent heat of solidification = 109 cal/g.

Modeling and Optimization of Motor Mount Bracket

Since a compatible electronic geometry description of the die was not available, a 3-D model of the die was constructed using ProEngineer™ software. The 3-D CAD information was then transferred to MeshCAST™, an automatic-mesh generation package, and the die and die cavity was meshed with tetrahedral elements. The final configuration contained approximately 96,000 elements and 21,000 nodes. ProCAST™ software was used for the mold filling and solidification modeling. Both color prints and a video animation of the results were produced. The modeling of the die filling and part solidification provided the following information:

1. The filling results indicated a propensity for air entrapment, particularly in the top cavity, suggesting that the gating system could be redesigned for smoother filling.
2. The solidification model indicated that the bottom cavity as well as the gate areas was likely to start solidifying before the top cavity.
3. The solidification results indicated that the likely region for porosity formation was the center of the bracket.
4. The filling and solidification model indicated that portions of the cavity attained a solid fraction of 40% about 5 s after the start of filling and that solidification was completed at the end of 35 s.

Figure 14 shows a velocity contour map of the filling of the die cavity 1.2 s after the start of filling. The results clearly illustrate the jetting of the molten metal into the top cavity, likely giving rise to oxide and air entrapment and the resulting severe surface defects obtained in castings in the top cavity. Closer examination of the defect pattern on the casting indicated that the outline of the surface defects matched the flow lines of the metal jet into the top cavity. It was also concluded that the dishing-in of the surface was probably an indication of solidification shrinkage due to improper compression.

Based on the results of the mold filling simulation, the gate areas were enlarged to allow a smoother flow of metal into the die cavity. Also, it was decided not to use the top cavity due to the excessive turbulence in this cavity. Since solidification of the bottom cavity commenced before the top cavity, it was decided to start compression before the onset of coherency (assumed to be at 40% solid) of the material in the bottom cavity. This ensured that compression would not be resisted by the solidifying material and could be used to compensate for solidification shrinkage.

The measured thermophysical properties of the die material were used to calculate the extent of die movement required to compensate for solidification shrinkage. The LTE of the die material as a function of temperature was measured. This information proved vital as it was discovered that the thermal expansion of the dies over several casting cycles negated much of the effect of the die movement required to compensate for solidification shrinkage. The knowledge of the LTE of the die was used to calculate the position of the dies after several casting cycles and then correctly calculate the required die movement to compensate for solidification shrinkage. Figure 15 shows a temperature

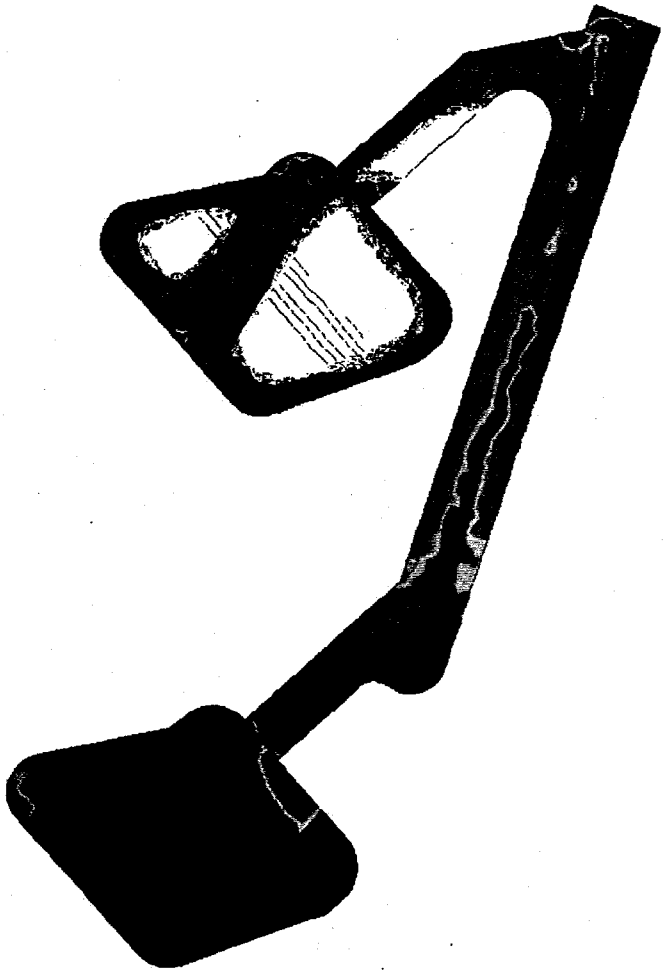

Figure 14. Velocity contour plot of the initial gating design 1.2 seconds after the start of filling, indicating jetting of molten metal into the top cavity.

contour map of the redesigned die cavity about 5 s after the start of filling indicating the onset of coherency in the gate area of the bottom cavity. Figure 15 also indicates the modified gating used in the final die design.

Prototypes of the motor mount bracket were successfully produced using the bottom cavity and information on the position and extent of die movement needed to compensate for solidification shrinkage. Figure 16 shows a picture of a completely sound motor mount bracket produced after process optimization. X-ray radiographs confirmed that the bracket was sound.

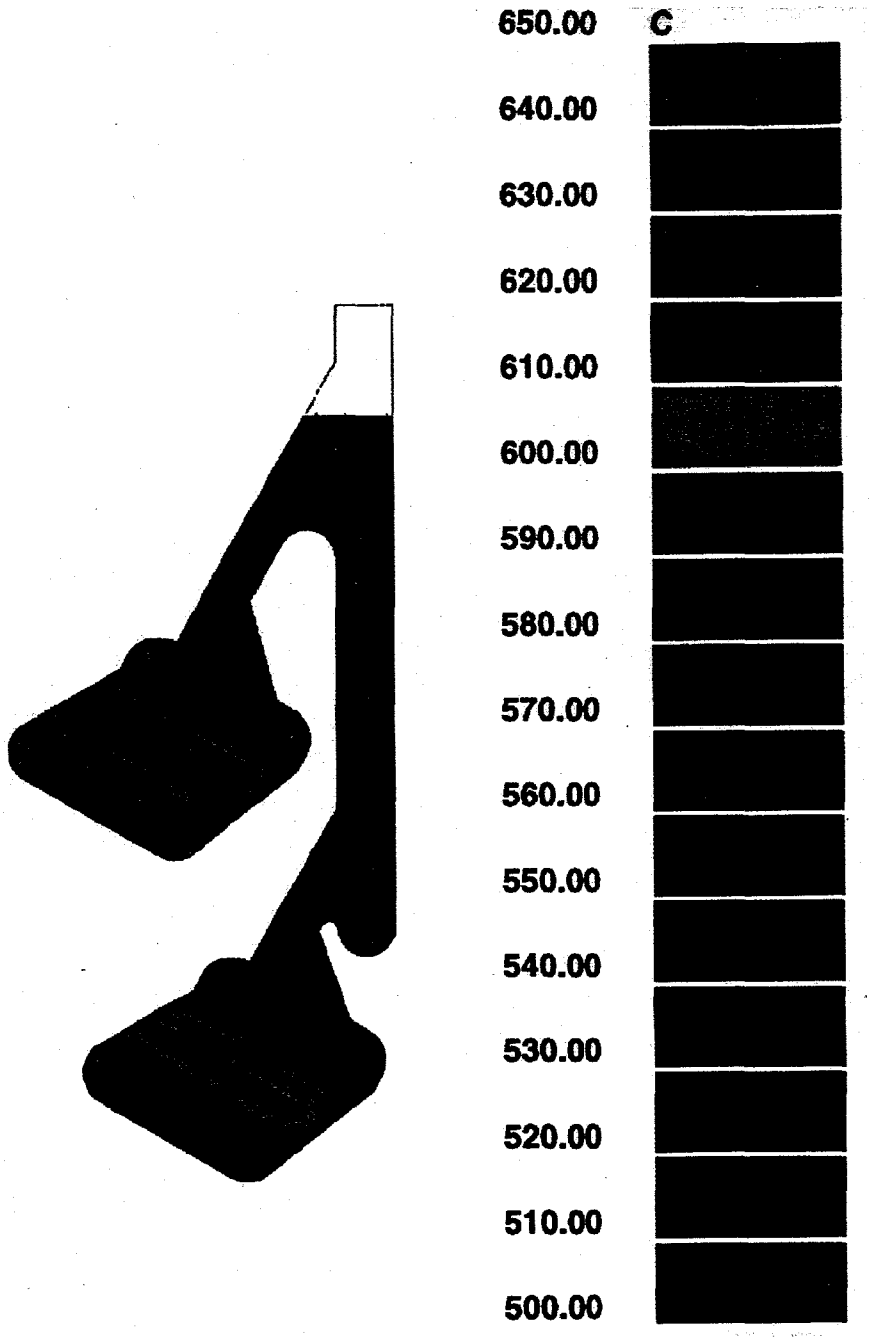

Figure 15. Temperature contour plot of the modified design 5 seconds after the start of filling, indicating the onset of coherency in the gate area of the bottom cavity.

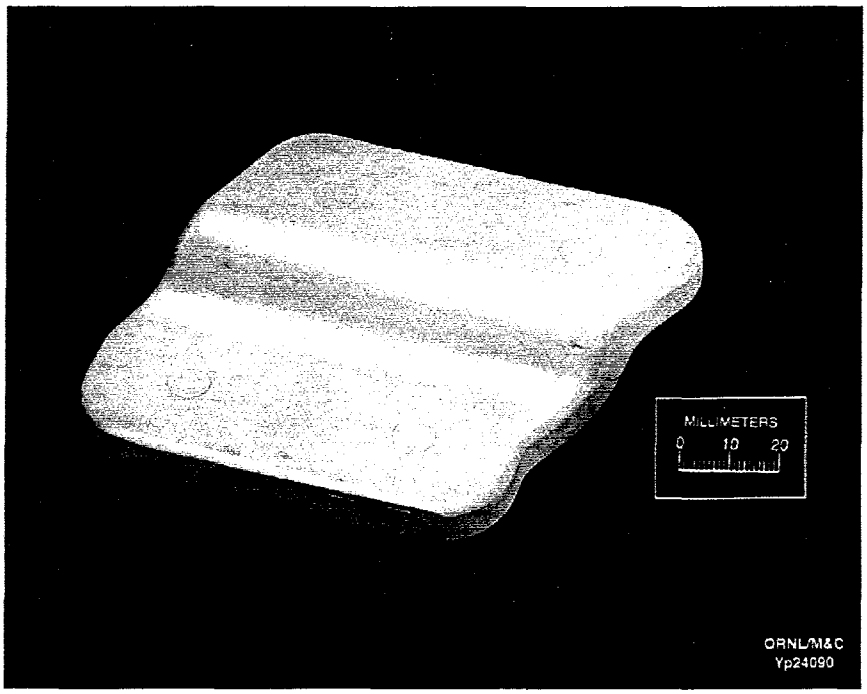

Figure 16: Completely sound motor mount MCF bracket produced after process optimization.

5.5 Tensile and Fatigue Properties of Optimized Motor Mount Bracket

Specimens for tensile and fatigue tests were obtained from motor mount brackets of aluminum 357 alloy heat treated to the T6 condition. The specimens had a uniform gage length of 1.5 cm with an overall length of 6.7 cm and were approximately 0.5 cm diam. The specimens exhibited an average yield strength of 276 MPa (40 ksi), ultimate tensile strength of 356 MPa (51.6 ksi), and total elongation of 12.3% at room temperature, and an average yield strength of 249 MPa (36.1 ksi), ultimate tensile strength of 296 MPa (42.9 ksi), and total elongation of 8.3% at 121°C (250°F). The properties compare well with the published[1] properties for wrought aluminum 6061 alloy at room temperature in the T6 condition - 275 MPa (40 ksi) yield strength, 310 MPa (45 ksi) ultimate tensile strength, and 17% elongation for 0.5-in.-diam specimens with a 5-cm (2-in.) gage length. The difference in the elongation value may be partly attributed to the difference in specimen dimensions. Figure 17 summaries the measured tensile properties of the motor mount bracket. Figures 18 and 19 show the measured fatigue properties for specimens from the MCF motor mount bracket. The fatigue strengths at room temperature and 250°F are very similar. The material exhibits excellent high cycle-fatigue strength although considerable data scatter is apparent. Importantly, the fatigue properties obtained from the bracket significantly exceeded the design requirements for the part.

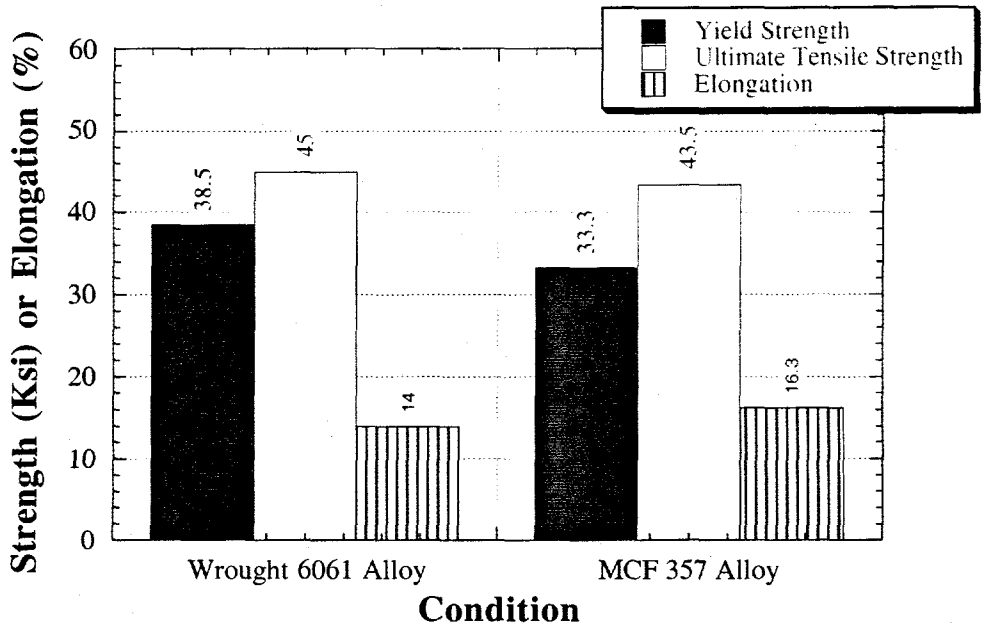

Figure 17. Tensile properties of 357 alloy motor mount compared to that of published data for wrought 6061 alloy [1].

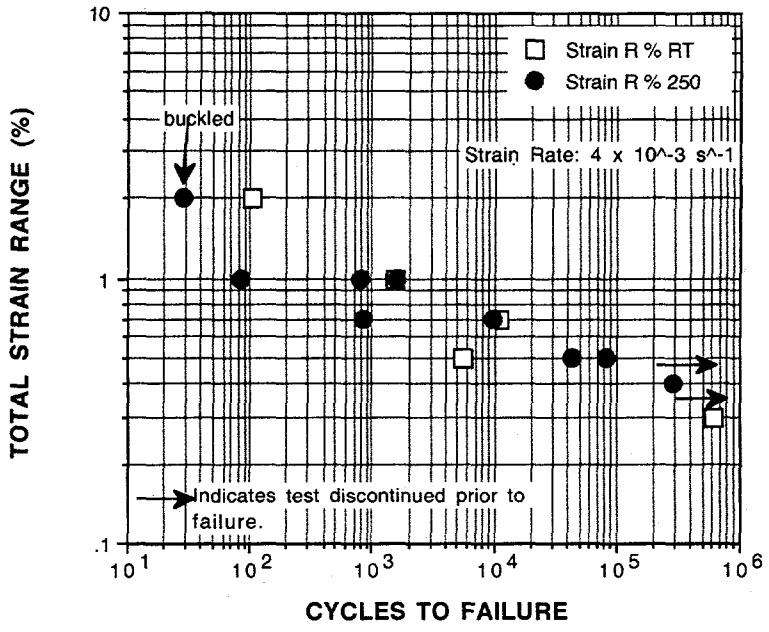

Figure 18: Fatigue life comparisons for strain controlled fatigue tests of MCF motor mount specimens at room temperature and 121°C (250°F).

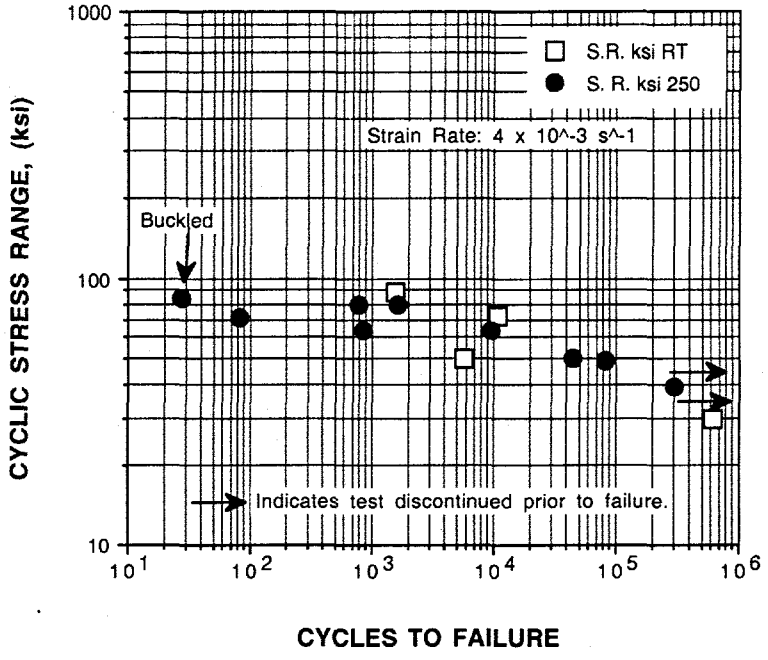

Figure 19: Stress range at half cycle life versus cycles to failure for strain controlled fatigue tests of MCF motor mount specimens at room temperature and 121°C (250°F).

The reason for the scatter in the tensile and fatigue data was investigated. The fracture surfaces of tensile and fatigue samples were examined in a SEM. There was clear evidence of microporosity on the fracture surfaces (see Figure 20). Note that the levels of microporosity on the fracture surfaces are considerably greater than that observed on a metallographic section, since the fracture path tends to seek out planes of weakness. The reasons for microporosity in the motor mount samples may be: (1) improper shut-off of cavity resulting in a loss of pressure during the squeeze, (2) the use of too low a squeeze pressure, and/or (3) high level of hydrogen in the melt.

The presence of microporosity on the fracture surfaces suggests that careful optimization of the MCF process should be carried out for each part, since process parameters are likely to vary with part geometry and alloy composition. The modeling of microporosity formation during the MCF process should be able to identify conditions that minimize microporosity, and consequently reduce or eliminate scatter in property data. Although commercial casting simulation software cannot typically model microporosity formation, a code with this capability has been recently developed at ORNL [2].

Figure 20. SEM micrograph of a fracture surface from a 357 alloy MCF motor mount sample indicating the presence of microporosity.

5.6 Analysis and Development of the MCF Process for MMC alloys

The development of the MCF process for a Duralcan MMC alloy containing 20-vol % of SiC particulate was carried out in a manner similar to the development of the A356 alloy motor mount bracket. The tasks involved included:

1. melting and casting of the MMC alloy in the laboratory,
2. measurement of thermophysical properties of the MMC alloy,
3. modeling of the filling and solidification behavior of the MMC alloy,
4. melting and casting of motor mount brackets at TAC facilities,
5. measurement of tensile properties of the MMC alloy.

5.6.1 Melting and Casting of Laboratory Samples of MMC Alloy: Since the MMC alloy contains 20-vol % of SiC particulate, it must be melted and handled somewhat differently than a monolithic aluminum alloy. Most importantly, it is necessary to continuously stir the alloy during melting to prevent settling of the SiC particulate. Accordingly, a laboratory study was carried to assess the melting and casting behavior of the Duralcan MMC alloy.

A small resistance furnace of approximately 8-lb capacity was used for the melting and casting studies. A graphite rotor was fabricated for stirring the alloy during melting. The graphite rotor was attached to a motor and fixed to a movable stand such that it could be immersed into the melt when necessary. The Duralcan MMC alloy was provided to ORNL in the form of an ingot. The ingot was crushed into several pieces to fit the dimensions of the crucible used for melting. An argon blanket was used during melting. Once the alloy was molten, the stirrer was introduced into the melt to prevent settling of the SiC particulate. The Duralcan MMC alloy behaved in a manner very similar to a monolithic aluminum alloy with the exception of the use of a stirrer. This indicates that much of the same equipment that is used for aluminum melting can be used for the melting of the Duralcan alloy. Figure 21 shows an optical micrograph of a sample from the as-received Duralcan alloy ingot. The micrograph indicates that the SiC particulate is fairly fine (approximately 10 μm in size) and well dispersed throughout the ingot microstructure. No porosity or other defects were visible in the ingot sample.

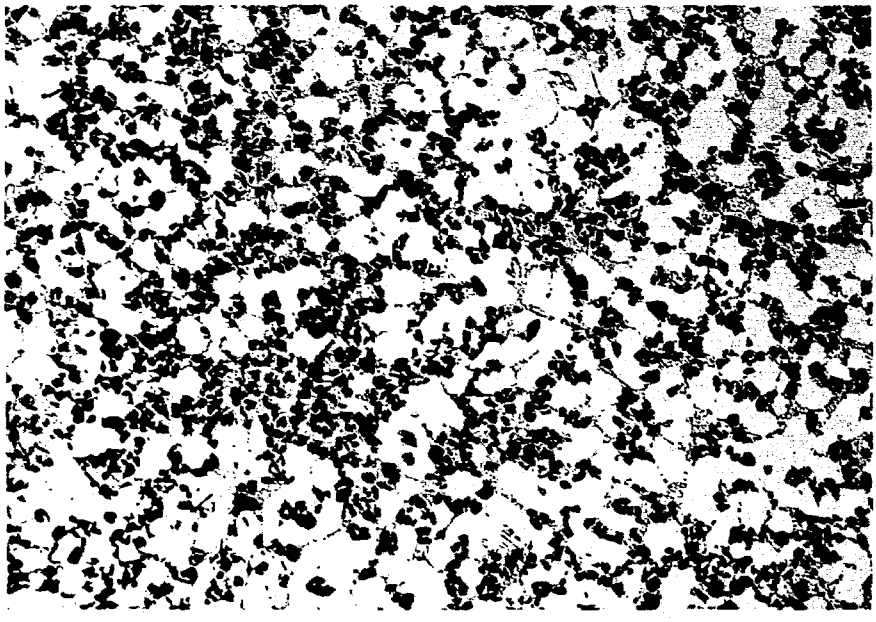

Figure 21. Optical micrograph (100×) of sample from the as-received Duralcan MMC alloy ingot, revealing the presence of well-dispersed SiC particulate.

The first melt was poured immediately after melting into a 2-cavity permanent mold tensile bar die that produced two standard ASTM 0.505 in. diam, 2-in. gauge length tensile bars. One of the tensile bars had a lap defect in the gauge length but the other tensile bar was optically defect-free. A metallographic specimen was taken from the gauge length of this tensile bar. Figure 22 shows an optical micrograph of the sample taken from the gauge length of the tensile bar. The micrograph of the test bar indicates

the presence of gross porosity in the sample. Figure 23 shows a SEM micrograph of a pore in the same sample, indicating the presence of particulate around and inside the pore. This suggests that the porosity is most likely due to entrapped air bubbles generated during the stirring of the molten alloy, since porosity generated during solidification will typically contain dendrites exposed due to the shrinkage and subsequent disappearance of the interdendritic liquid.

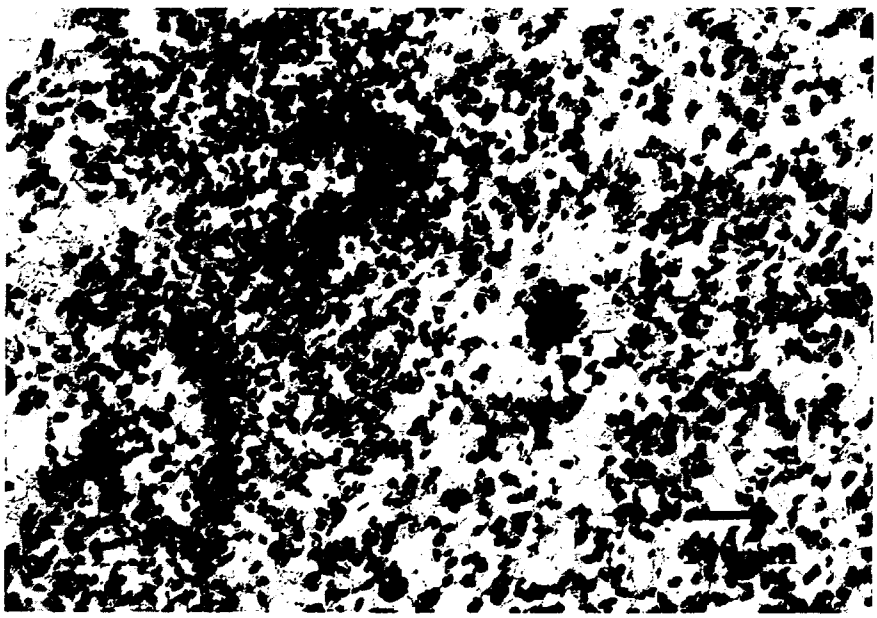

Figure 22. Optical micrograph of Duralcan MMC alloy sample from a test bar poured prior to degassing of the melt, indicating the presence of gross porosity.

The presence of gross porosity in the test bar indicated that the melt would need to be degassed after melting. Accordingly, an argon-10% chlorine gas mixture was introduced through a graphite lance into another melt of the Duralcan alloy, a procedure similar to that used for A356 alloy. The gas produced a severe reaction with the melt, resulting in the formation of a large amount of dark colored dross. Close examination of the dross indicated that that the dross contained a large amount of SiC particulate. This melt was discarded as it was apparent that the degassing procedure resulted in an extensive loss of the SiC particulate. A third melt of the Duralcan alloy was made, and the melt was degassed with plain argon gas. This time, the degassing procedure resulted in the formation of far less dross, although the amount of dross was still somewhat more than in the case of A356 alloy. This melt was also poured into the tensile bar mold. Figure 24 shows an optical micrograph of a sample from a degassed melt of Duralcan MMC alloy. It indicates that porosity persists even after degassing of the melt.

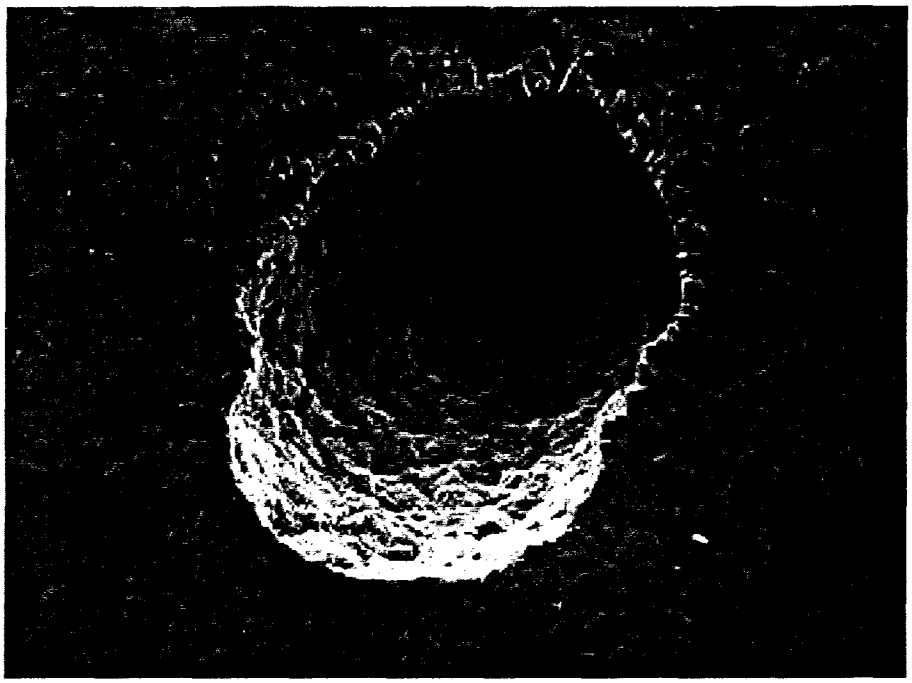

Figure 23. SEM micrograph of pore in Duralcan MMC alloy sample from a test bar poured prior to degassing of the melt, indicating that the porosity is most likely due to entrapped bubbles surrounded by SiC particulate.

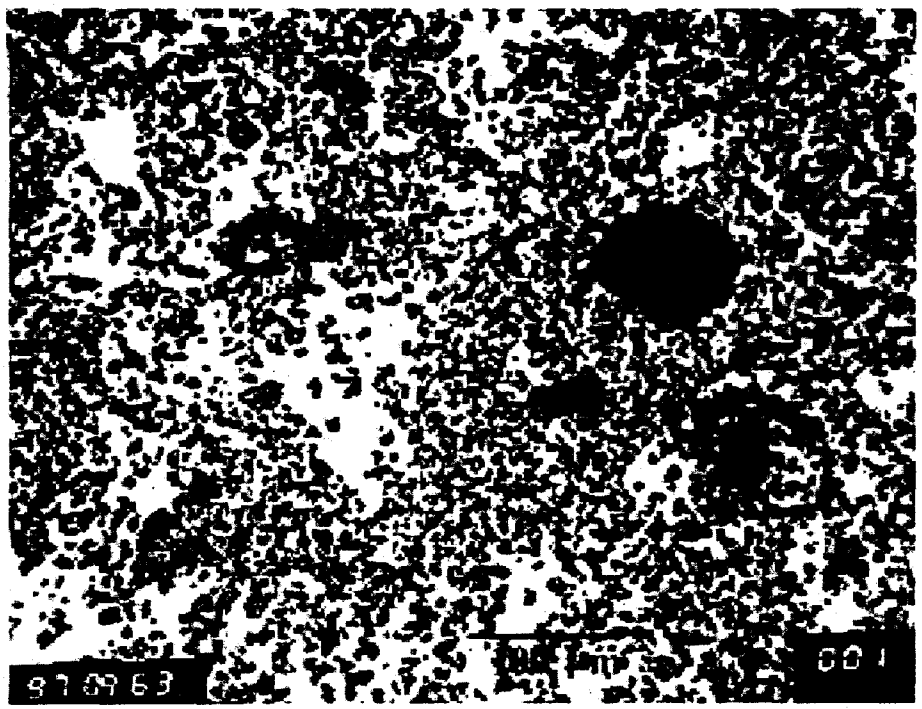

Figure 24. Optical micrograph of Duralcan MMC alloy sample from a test bar poured after degassing of the melt, indicating that porosity persists after degassing.

5.6.2 Measurement of Thermophysical Properties: Thermophysica l properties of the Duralcan MMC alloy were measured to analyze the mold filling behavior of the alloy. In addition to the themophysical properties measured for A356 alloy, the viscosity of the alloy was also measured. This was necessary as the viscosity of the MMC alloy is very different from that for a monolithic aluminum alloy due to the presence of the SiC particles. Table 2 lists the thermophysical properties of the MMC Duralcan alloy measured at the facilities of the HTML. Figure 25 lists the measured viscosity of the Duralcan MMC alloy as a function of temperature.

Table 2. Measured thermophysical properties for aluminum 356 alloy used in modeling

Temperature (°C)	Thermal Conductivity (W/m/K)	Density (g/cc)	Specific Heat (KJ/Kg/K)
25		2.76	
100	147.38		0.854
150	152.55		0.910
200	155.28		0.953
250	156.29		0.989
300	156.03		1.018
350	154.82		1.043
400	152.88		1.064
450	150.37		1.082
500	147.41		1.098
555	143.74	2.67	1.113
615		2.56	
800		2.51	

Latent Heat of Solidification = 83 cal/g

5.6.3 Modeling of Mold Filling and Solidification of MMC Alloy: The mold filling and solidification of the Duralcan MMC alloy motor mount bracket was modeled using ProCAST™ software, using the measured properties of the alloy. Although there was some difference in the filling behavior of the alloy compared to A356 alloy, the difference was not great enough to require any changes to the die design. Accordingly, the same MCF process parameters as those used for the A356 alloy were used for the production of MMC motor mount brackets.

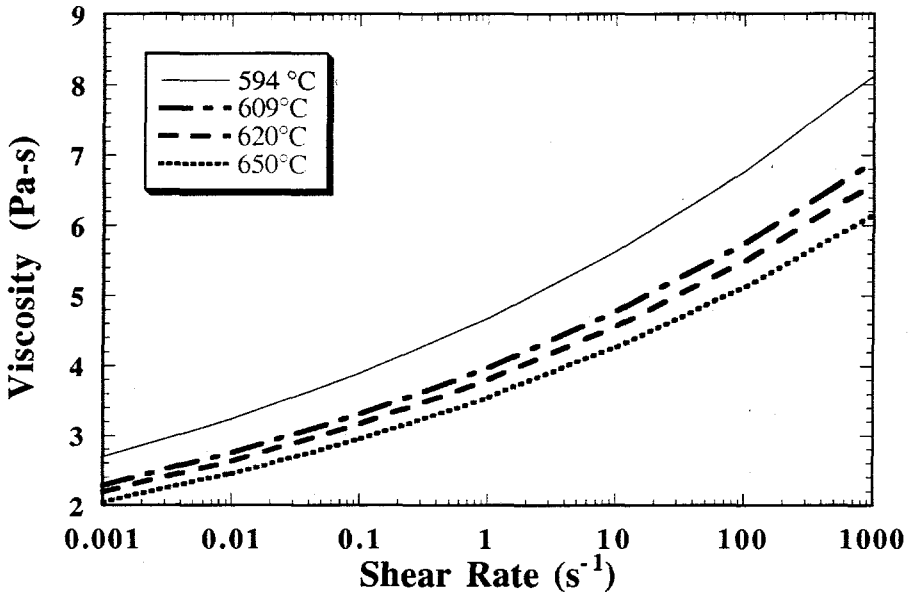

Figure 25. Measured viscosity of Duralcan MMC alloy as a function of temperature.

5.6.4 Tensile Properties of Duralcan MMC Alloy Motor Mount Bracket: Duralcan MMC alloy motor mount brackets received from TAC were tested in the T6 condition using a procedure identical to those used for the 357 alloy brackets. The specimens exhibited an average yield strength of 230 MPa (33.3 ksi), ultimate tensile strength of 250 MPa (36.2 ksi), and total elongation of 0.55% at room temperature, compared with an average yield strength of 276 MPa (40 ksi), ultimate tensile strength of 356 MPa (51.6 ksi), and total elongation of 12.3% exhibited by the 357 alloy specimens. The lower total elongation exhibited by the Duralcan MMC alloy is expected due to the presence of the SiC reinforcement. However, it is instructive to check for the presence of defects, in order to assess opportunities for the improvement and optimization of properties.

Optical and SEM micrographs were obtained of the microstructure of the bracket and the fracture surfaces of tensile specimens. Figure 26 shows an optical micrograph of a Duralcan MMC alloy MCF motor mount sample. It exhibits well-dispersed SiC particles and an absence of gross porosity, indicating that the MCF process is successful at closing entrapped bubbles. However, SEM micrographs of the fracture surface reveal the presence of a number of oxide films (see Figures 27 and 28). It is likely that these oxide films are largely responsible for the poor ductility exhibited by the MCF samples. Consequently, it appears that much greater care needs to be taken during the pouring to avoid the formation of oxide films.

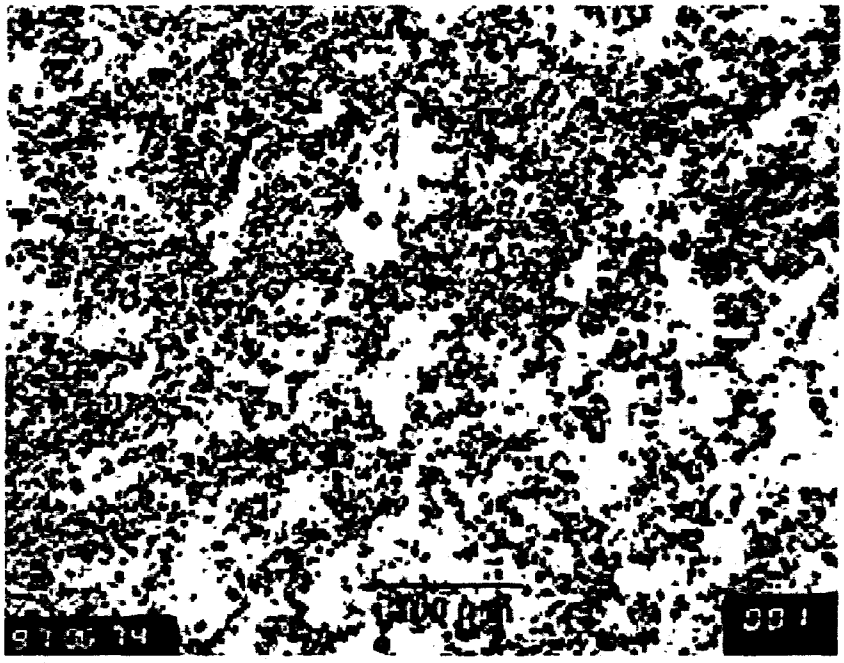

Figure 26. Optical micrograph of Duralcan MMC alloy MCF motor mount sample indicating the absence of gross porosity.

Figure 27. SEM micrograph of the fracture surface of Duralcan MMC alloy MCF motor mount sample indicating the presence of a large number of oxide films.

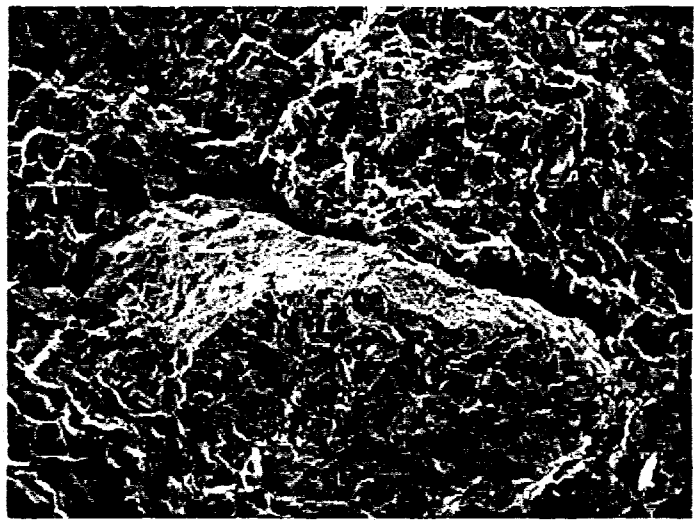

Figure 28. SEM micrograph of the fracture surface of Duralcan MMC alloy MCF motor illustrating that oxide films provide preexisting cracks that promote failure, resulting in a low ductility of the sample.

6.0 SUMMARY AND CONCLUSIONS

A new process called Metal Compression Forming, a variant of the squeeze casting process, was successfully used to produce prototype aluminum 357 alloy motor mount brackets. The MCF process can use low-pressure bottom-filling to allow the filling of the mold cavity in a quiescent manner and avoid the formation of trapped gas pockets and oxide films. In addition, the MCF process applies pressure on the entire mold face, thereby directing pressure uniformly on all regions of the casting and producing a uniformly sound part.

The determination of thermophysical properties for the alloy, especially the density variation across the freezing range and the linear thermal expansion of the die material, as well as the use of casting and solidification models of the filling of the die cavity and the solidification of the part, were crucial to the development of optimum process parameters for the production of a sound part. The measured properties were vital to both casting modeling and for calculations of the extent of die movement required to compensate for solidification shrinkage. Prototypes of the motor mount bracket were successfully made based on information obtained from the casting modeling and information on the position and extent of die movement needed to compensate for solidification shrinkage. Tensile and fatigue properties of samples compared favorably with that of wrought aluminum 6061 alloy and significantly exceeded the design requirements for the part.

The results of the mold filling simulation illustrated the rapid acceleration of the metal stream during gravity assisted pouring, and emphasized the importance of approaches such as low-pressure bottom-filling to ensure a quiescent filling of metal and prevent the generation and incorporation of oxide films in the casting. An added advantage of the

low-pressure bottom-filling approach is that excess metal may be allowed to return to the holding furnace when pressure is released, thereby providing increased metal yields. Table 2 illustrates the salient features of the MCF process as contrasted with high pressure die casting and indirect squeeze casting for the production of safety critical structural aluminum alloy castings.

Table 2. Salient features of the MCF process as contrasted with high-pressure die casting and indirect squeeze casting

Condition	High Pressure Die Casting	Indirect Squeeze Casting	Metal Compression Forming
Pressure	No Pressure During Solidification	Nonuniform Pressure	Uniform Pressure
Filling	Highly Turbulent	Less Turbulent	Quiescent
Inclusions	Lots of Inclusions	Some Inclusions	No Inclusions
Porosity	High Porosity	Some Porosity	No Porosity
Properties	Poor Properties	Nonuniform Properties	Properties Comparable to Forging
Metal Yield	50-60%	50-60%	80-90%

The commercial version of the process will use a low-pressure bottom fill approach rather than the tilt pour arrangement. The process shows promise for the manufacture of metal matrix composite materials and other alloys such as aluminum 6061 alloy. However, development of improved metal transfer techniques will be needed to prevent the settling of particulate and the entrapment of gas bubbles during the casting of MMC alloys.

Inventions

No inventions were made or reported regarding this CRADA. However, results of the modeling provided the impetus for the use of a low-pressure bottom fill approach for the commercial version of the process. Also, the interaction between ORNL and TAC raised possibilities for the use of other ORNL technologies, such as improved mold materials and die coatings.

Commercialization and Future Work

This CRADA clearly demonstrated that the MCF process can be used for the production of very high integrity structural aluminum alloy castings with properties comparable to forgings. The technologies demonstrated in this CRADA are well suited for application to commercial casting production. In fact, based on the results of this CRADA, a commercialization program is already underway at TAC. Another proof of the future viability of the MCF process is the fact that it was awarded an R & D 100 Award by *R & D Magazine* in 1997, recognizing it as one of the 100 most technologically significant new products of the year. Future plans for collaboration include the continuation of this work either informally or through continuing funding from this or other programs.

Acknowledgments

The authors would like to thank E. C. Hatfield for melting and casting, C. O. Stevens for conducting tensile and fatigue tests, H. F. Longmire and J. R. Mayotte for metallography, and M. L. Atchley for preparing the manuscript.

This research was sponsored by the U.S. Department of Energy, Assistant Secretary for Energy Efficiency and Renewable Energy, Office of Transportation Technologies, Office of Heavy Vehicle Technology, under contract DE-AC05-96OR22464 with Lockheed Martin Energy Research Corp.

References

1. ASM Specialty Handbook, Aluminum and Aluminum Alloys, Materials Park, Ohio, ASM International, 1993, p 72.

2. S. Viswanathan, A. S. Sabau, Q. Han, and A, J. Duncan, "Modeling of Porosity in Aluminum Alloy Castings," Advances in Aluminum Casting Technology, eds. M. Tiryakioglu and J. Campbell, Materials Park, Ohio, ASM International, 1998, p 135.

INTERNAL DISTRIBUTION

1. E. E. Bloom
2. R. A. Bradley
3. C. R. Brinkman
4-5. D. R. Hamrin
6. Q. Han
7. E. C. Hatfield
8. T. J. Huxford
9. A. J. Luffman
10. W. D. Porter
11. A. S. Sabau
12. V. K. Sikka
13. P. S. Sklad
14. C. A. Valentine
15-16. S. Viswanathan

EXTERNAL DISTRIBUTION

17-19. Thompson Aluminum Casting Co., Inc., 4850 Chaincraft Road, Cleveland, OH 44125
R. M. Purgert
J. Thomas

20-21. TTE Die Casting, Inc., 1017 Alvin Weinberg Drive, Oak Ridge, TN 37830
B. Edney
G. Palmer

22. DOE, EE-33, 1000 Independence Avenue, SW, Washington, DC 20585
S. Diamond

23-24. Office of Scientific and Technical Information, P.O. Box 62, Oak Ridge, TN 37831

25. DOE, Oak Ridge Operations, P.O. Box 2008, Oak Ridge, TN 37831-6269
P. L. Gorman

26. DOE-WFO, MS G209